# Decomposition of the point-dipole field into homogeneous and evanescent parts

T. Setälä and M. Kaivola

*Helsinki University of Technology, Materials Physics Laboratory, FIN-02150 Espoo, Finland*

A. T. Friberg

*Royal Institute of Technology, Department of Physics II–Optics, S-100 44 Stockholm, Sweden*

In near-field optics the resolution and sensitivity of measurements depend on the abundance of evanescent waves in relation to propagating waves. The electromagnetic field propagator is related to the scalar spherical wave, for which the Weyl expansion is a half-space representation containing both evanescent and homogeneous plane waves. Making use of these results, we decompose the dyadic free-space Green function into its evanescent and homogeneous parts and show that some approaches put forward in the literature are inconsistent with this formulation. We express the results in a form that is suitable for numerical computation and illustrate the field decomposition for a point dipole in some typical cases. [S1063-651X(99)05001-1]

PACS number(s): 41.20.Jb, 07.79.Fc

## I. INTRODUCTION

In the past few years near-field optical microscopy (SNOM or NSOM) has become an important practical tool to acquire information about the optical properties of matter in the nanometer scale [1,2]. The near-field technique allows the classical diffraction limit to be surpassed typically by an order of magnitude. It is generally accepted that in near-field optics the high spatial resolution is obtained through detection of the evanescent (or nonradiating) electromagnetic field which concentrates near the sample surface. However, the question of how the nanoscale information is stored in the evanescent field is rather complicated [3]. In any case the sensitivity of a near-field measurement strongly depends on the ratio of this evanescent field to the homogeneous (or propagating) component that is always present.

A careful analysis of the signal detected in near-field measurement requires a fully electromagnetic treatment of the optical fields involved. Useful insight into the problem can be gained by considering a point dipole and by decomposing the associated free-space dyadic Green function into its propagating and nonpropagating constituents. An analogous decomposition has previously been discussed for the case of the scalar spherical wave [4,5]. In Ref. [5] an expression in terms of Bessel and Lommel functions was found for the evanescent field contribution. Recently, a closed-form formula for the evanescent dyadic Green function was suggested and extensively used in SNOM simulations [6].

In this paper we decompose the scalar and dyadic free-space Green functions into their homogeneous and evanescent parts on the basis of proper half-space field representations. The results are expressed in a compact form that is suitable for efficient numerical computations. We comment on the nature of the decompositions and illustrate the point-source and point-dipole field components in some characteristic situations. Our expressions for the evanescent-wave and homogeneous-wave dyadic Green functions differ in general from those in Refs. [6]; they agree only in one given direction and we conclude that the method employed in those works is incorrect.

## II. DIPOLE FIELD

We consider a point dipole **P** located in the origin, generating a monochromatic field which at an arbitrary observation point **r** can be written (in SI units) as

$$\mathbf{E}(\mathbf{r}) = \frac{\mu_0 \omega^2}{4\pi} \, \overleftrightarrow{G}(\mathbf{r}) \cdot \mathbf{P}. \tag{2.1}$$

Here $\mu_0$ is the permeability of the vacuum, $\omega$ is the angular frequency of the light, and $\overleftrightarrow{G}(\mathbf{r})$ is the dyadic free-space Green function. This function contains all the information about the field components created by the source dipole pointing in an arbitrary direction. The dyadic Green function is expressible as [7]

$$\overleftrightarrow{G}(\mathbf{r}) = \left( \overleftrightarrow{U} + \frac{1}{k^2} \boldsymbol{\nabla}\boldsymbol{\nabla} \right) G(\mathbf{r}), \tag{2.2}$$

where $\overleftrightarrow{U}$ is the unit dyadic, $k = \omega/c = 2\pi/\lambda$ is the wave number of the field, and $c$ is the speed of light in vacuum. The function $G(\mathbf{r}) = \exp(ikr)/r$ is the outgoing scalar free-space Green function which satisfies the inhomogeneous Helmholtz equation with a $\delta$-function source term in the origin. On performing the derivations, Eq. (2.2) may also be written in the form

$$\overleftrightarrow{G}(\mathbf{r}) = \left[ \left( \frac{1}{r} + \frac{i}{kr^2} - \frac{1}{k^2 r^3} \right) \overleftrightarrow{U} \right.$$
$$\left. + \left( -\frac{1}{r} - \frac{3i}{kr^2} + \frac{3}{k^2 r^3} \right) \mathbf{r}_0 \mathbf{r}_0 \right] \exp(ikr), \tag{2.3}$$

where $\mathbf{r}_0$ is a unit vector in the **r** direction.

The objective of this paper is to decompose the total field given by Eq. (2.1), and accordingly the dyadic Green func-
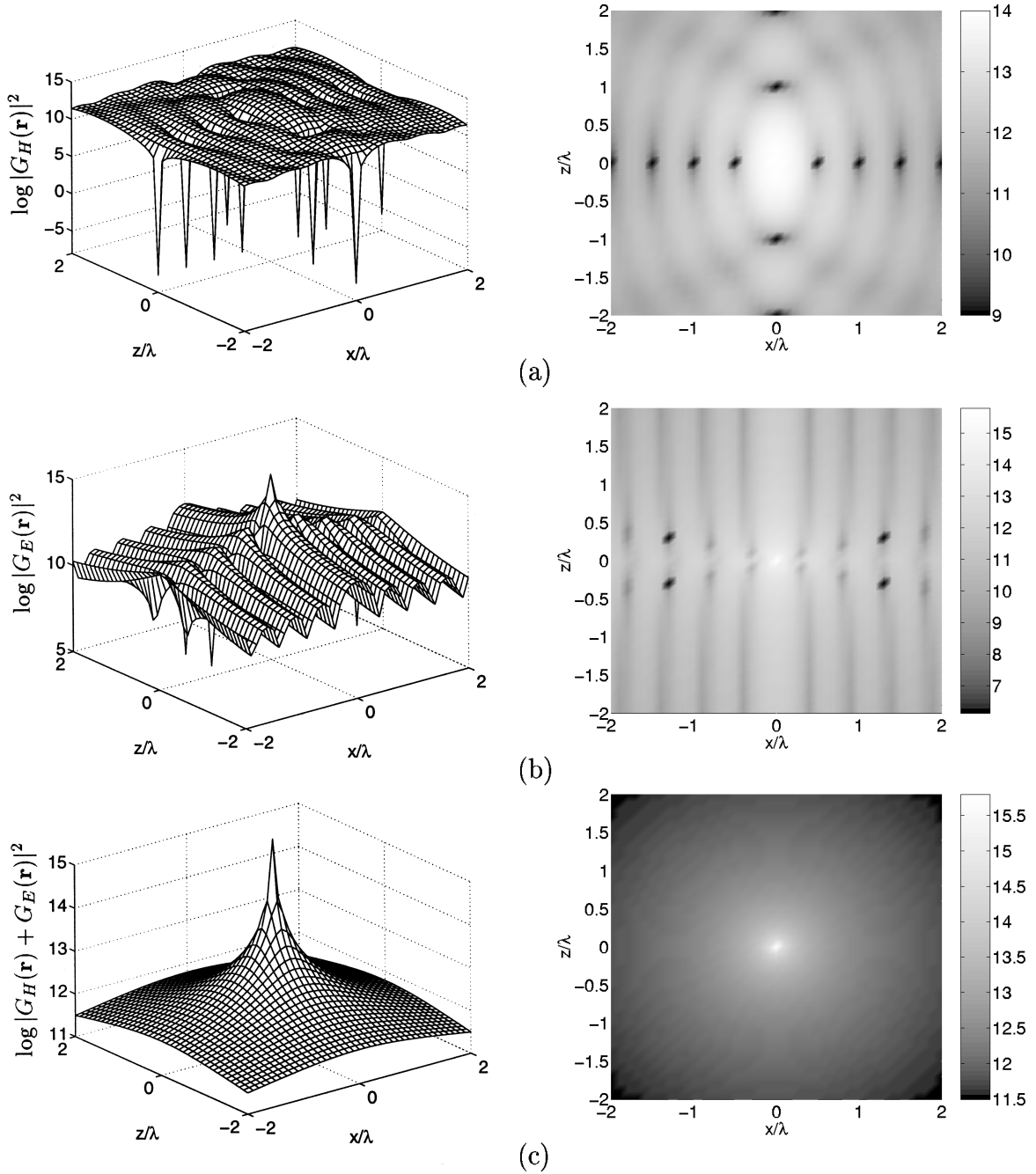
         

(a)

(b)

(c)

FIG. 1. Logarithmic ($\log_{10}$) intensity distributions of the field in the plane $y=0$, generated by a unit scalar point source located in the origin. (a) Homogeneous part, (b) evanescent part, (c) total field. The results have been calculated for $\lambda = 633$ nm.

tion of Eq. (2.2), into the homogeneous and evanescent parts. In order to do this, we first consider the corresponding decomposition of the scalar function $G(\mathbf{r})$ in source-free half-spaces.

## III. DECOMPOSITION OF THE SCALAR SPHERICAL WAVE

The scalar spherical wave field $G(\mathbf{r})$, created by a point source in the origin, satisfies the homogeneous scalar Helmholtz equation in the source-free half-spaces $z>0$ and $z<0$. It is convenient to express this wave field in an integral representation which is composed as a superposition of ho-

mogeneous plane waves propagating in the various directions and of exponentially decaying, nonpropagating, evanescent plane waves. This angular-spectrum representation, known as the Weyl expansion, can be written as [8]

$$G(\mathbf{r}) = \frac{ik}{2\pi} \int \int_{-\infty}^{\infty} \frac{1}{m} \exp[ik(px+qy+m|z|)]dp\,dq,$$

(3.1)

where

$$m = \sqrt{1-p^2-q^2} \quad \text{for } p^2+q^2 \leqslant 1,$$

(3.2)

$$m = i\sqrt{p^2 + q^2 - 1} \quad \text{for } p^2 + q^2 > 1. \qquad (3.3)$$

The scalar field $G(\mathbf{r})$ of Eq. (3.1) can be expressed as a sum of two double integrals

$$G(\mathbf{r}) = G_H(\mathbf{r}) + G_E(\mathbf{r}), \qquad (3.4)$$

where

$$G_H(\mathbf{r}) = \frac{ik}{2\pi} \int \int_{p^2 + q^2 \leqslant 1} \frac{1}{m}$$
$$\times \exp[ik(px + qy + m|z|)]dp\,dq, \qquad (3.5)$$

$$G_E(\mathbf{r}) = \frac{ik}{2\pi} \int \int_{p^2 + q^2 > 1} \frac{1}{m}$$
$$\times \exp[ik(px + qy + m|z|)]dp\,dq. \qquad (3.6)$$

The function $G_H(\mathbf{r})$ contains all the propagating plane waves and is therefore called the homogeneous part of the field. Similarly, the function $G_E(\mathbf{r})$ contains all the exponentially decaying plane waves and is called the evanescent part.

The functions $G_H(\mathbf{r})$ and $G_E(\mathbf{r})$ can be expressed in a closed form in two special cases, namely along the chosen $z$ axis and in the plane $z = 0$. However, it appears that there is no closed-form solution to these functions in an arbitrary direction and the integrals have to be calculated numerically. On making use of the polar coordinates for the integration variables and performing simple changes in the radial integration variable, the functions $G_H(\mathbf{r})$ and $G_E(\mathbf{r})$ may be transformed into a form that is more suitable for numerical calculations, viz.,

$$G_H(\mathbf{r}) = ik \int_0^1 \exp[i\alpha(z)v]J_0[\beta(x,y)\sqrt{1 - v^2}]dv, \qquad (3.7)$$

$$G_E(\mathbf{r}) = k \int_0^\infty \exp[-\alpha(z)v]J_0[\beta(x,y)\sqrt{v^2 + 1}]dv. \qquad (3.8)$$

Here $J_0$ is the Bessel function of the first kind and order zero, the coordinate-dependent parameters $\alpha(z)$ and $\beta(x,y)$ have the form

$$\alpha(z) = k|z|,$$
$$\beta(x,y) = k\sqrt{x^2 + y^2}, \qquad (3.9)$$

and $v$ is the transformed radial integration variable.

Expressions (3.7) and (3.8) are cylindrically symmetric about the $z$ axis and mirror symmetric with respect to the $z = 0$ plane. These characteristics are also evident in Figs. 1(a) and 1(b), in which we have plotted $\log_{10}|G_H(\mathbf{r})|^2$ and $\log_{10}|G_E(\mathbf{r})|^2$ in the plane $y = 0$. Furthermore, the total field intensity calculated as the interference of the homogeneous and evanescent parts is spherically symmetric as expected [see Fig. 1(c) illustrating $\log_{10}|G(\mathbf{r})|^2$]. Figure 1(b) shows that the evanescent part (or the envelope of the ridges) decays slower in the direction of the $z$ axis and in the plane $z = 0$ than in any other direction. This observation is in accordance with the results presented earlier by Sherman *et al.* [9] and quite recently by Wolf and Foley [10].

It is important to note that when writing the Weyl expression, the whole space is divided into two source-free half-spaces separated by the plane $z = 0$. For point sources this division is quite arbitrary and could be made equally well using any other plane. Each choice of the dividing plane will, however, lead to different mathematical values for the homogeneous and evanescent parts in a given point. In all cases the evanescent plane waves will decay exponentially in the direction perpendicular to the dividing plane and they will propagate in directions parallel to that plane. Since all the different choices must be considered as correct, the physical meaning of the spherical-wave decomposition into its homogeneous and evanescent part is somewhat vague. We argue that the decomposition should be understood simply as a mathematical tool which becomes meaningful only when applied to a real physical situation in which the geometry of the problem fixes the orientation of the dividing plane.

## IV. DECOMPOSITION OF THE VECTOR FIELD

By taking advantage of the results of the preceding section, we decompose the vector field of the point dipole located at the origin into its homogeneous and evanescent parts. To accomplish this, we only need to divide the dyadic free-space Green function (2.2) into the respective parts since the corresponding field components are then obtained from Eq. (2.1).

On substituting the Weyl expansion (3.1) into Eq. (2.2), we find for the dyadic Green function $\overset{\leftrightarrow}{G}(\mathbf{r})$ the following angular-spectrum representation:

$$\overset{\leftrightarrow}{G}(\mathbf{r}) = \frac{ik}{2\pi} \int \int_{-\infty}^\infty \frac{1}{m} \overset{\leftrightarrow}{A}(p,q)$$
$$\times \exp[ik(px + qy + m|z|)]dp\,dq, \qquad (4.1)$$

where the dyad $\overset{\leftrightarrow}{A}(p,q)$ takes on the symmetric form

$$\overset{\leftrightarrow}{A}(p,q) = \begin{pmatrix} 1 - p^2 & -pq & \mp pm \\ -qp & 1 - q^2 & \mp qm \\ \mp mp & \mp mq & 1 - m^2 \end{pmatrix}. \qquad (4.2)$$

In Eq. (4.2), and from now on, the upper signs refer to the region $z \geqslant 0$ and the lower signs to the region $z < 0$. Note also the formal similarity of Eq. (4.1) with Eq. (3.1); they differ only by the presence of the dyad $\overset{\leftrightarrow}{A}(p,q)$. Performing the integration over the entire $k$ space, as indicated in Eq. (4.1), leads to expression (2.3).

Formally we could calculate the homogeneous ($p^2 + q^2 \leqslant 1$) and evanescent ($p^2 + q^2 > 1$) parts of the dyadic Green function, denoted by $\overset{\leftrightarrow}{G}_H(\mathbf{r})$ and $\overset{\leftrightarrow}{G}_E(\mathbf{r})$, respectively, by direct integration of Eq. (4.1). However, it is more convenient to determine these functions by substituting into Eq. (2.2) the forms (3.7) and (3.8), which still are in Cartesian coordinates but in which one integration already has been carried out. Unfortunately, it does not seem possible to perform analytically the remaining integral to find closed-form expressions for the homogeneous and the evanescent parts. These functions can, however, be expressed in a rather compact form containing only simple classes of integrals which can readily be computed numerically. By direct calculation we find for the homogeneous part

$$\overset{\leftrightarrow}{G}_H(\mathbf{r})=ik\begin{pmatrix} I_0^H+\dfrac{k^2(x^2-y^2)}{\beta^3}L_1^H-\dfrac{k^2x^2}{\beta^2}L_2^H & \dfrac{k^2xy}{\beta^2}\left[\dfrac{2}{\beta}L_1^H-L_2^H\right] & \mp\dfrac{ikx}{\beta}L_3^H \\[3mm] \dfrac{k^2xy}{\beta^2}\left[\dfrac{2}{\beta}L_1^H-L_2^H\right] & I_0^H+\dfrac{k^2(y^2-x^2)}{\beta^3}L_1^H-\dfrac{k^2y^2}{\beta^2}L_2^H & \mp\dfrac{iky}{\beta}L_3^H \\[3mm] \mp\dfrac{ikx}{\beta}L_3^H & \mp\dfrac{iky}{\beta}L_3^H & L_2^H \end{pmatrix}, \tag{4.3}$$

where

$$L_1^H(\mathbf{r})=\frac{i}{\alpha}[J_1(\beta)-\beta I_1^H],$$

$$L_2^H(\mathbf{r})=I_0^H-I_2^H, \tag{4.4}$$

$$L_3^H(\mathbf{r})=-\frac{1}{\beta}[J_0(\beta)+i\alpha I_0^H-2I_1^H-i\alpha I_2^H],$$

and

$$I_n^H(\mathbf{r})=\int_0^1 v^n e^{i\alpha(z)v}J_0[\beta(x,y)\sqrt{1-v^2}]dv. \tag{4.5}$$

For the evanescent part we find

$$\overset{\leftrightarrow}{G}_E(\mathbf{r})=k\begin{pmatrix} I_0^E+\dfrac{k^2(x^2-y^2)}{\beta^3}L_1^E-\dfrac{k^2x^2}{\beta^2}L_2^E & \dfrac{k^2xy}{\beta^2}\left[\dfrac{2}{\beta}L_1^E-L_2^E\right] & \pm\dfrac{kx}{\beta}L_3^E \\[3mm] \dfrac{k^2xy}{\beta^2}\left[\dfrac{2}{\beta}L_1^E-L_2^E\right] & I_0^E+\dfrac{k^2(y^2-x^2)}{\beta^3}L_1^E-\dfrac{k^2y^2}{\beta^2}L_2^E & \pm\dfrac{ky}{\beta}L_3^E \\[3mm] \pm\dfrac{kx}{\beta}L_3^E & \pm\dfrac{ky}{\beta}L_3^E & L_2^E \end{pmatrix}, \tag{4.6}$$

where

$$L_1^E(\mathbf{r})=\frac{1}{\alpha}[J_1(\beta)+\beta I_1^E],$$

$$L_2^E(\mathbf{r})=I_0^E+I_2^E, \tag{4.7}$$

$$L_3^E(\mathbf{r})=\frac{1}{\beta}[J_0(\beta)-\alpha I_0^E+2I_1^E-\alpha I_2^E],$$

and

$$I_n^E(\mathbf{r})=\int_0^\infty v^n e^{-\alpha(z)v}J_0[\beta(x,y)\sqrt{v^2+1}]dv. \tag{4.8}$$

In these equations $J_0$ and $J_1$ are Bessel functions and the parameters $\alpha(z)$ and $\beta(x,y)$ are the same as in the scalar case, given by Eq. (3.9).

The symmetry properties of the homogeneous and evanescent parts of the dyadic Green function are not as transparent as in the scalar case, and a general discussion of the symmetries based on Eqs. (4.3) and (4.6) necessarily becomes rather complicated. Formally the expressions (4.3) and (4.6) for the homogeneous and evanescent contributions look very similar, but both mathematically and physically

they are different. The physical implications are best seen by considering the homogeneous and evanescent parts of the point-dipole field.

The dyadic equations (4.3) and (4.6) are valid for any point dipole $\mathbf{P}$ at the origin, but for simplicity we take $\mathbf{P}=(0,0,1)$, i.e., a unit dipole pointing in the positive $z$ direc-
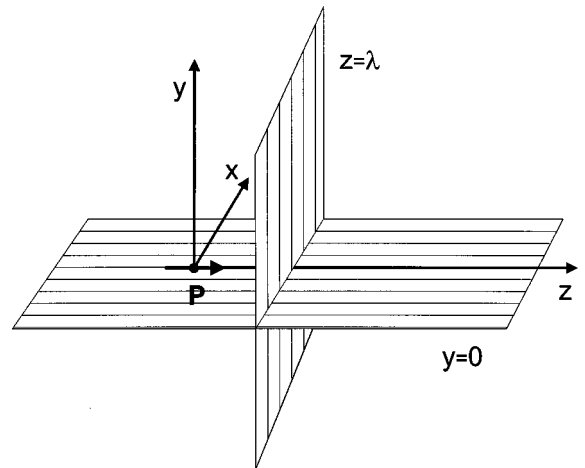


FIG. 2. Illustration of point dipole $\mathbf{P}=(0,0,1)$ located in the origin and the planes of observation at $z=\lambda$ and $y=0$.
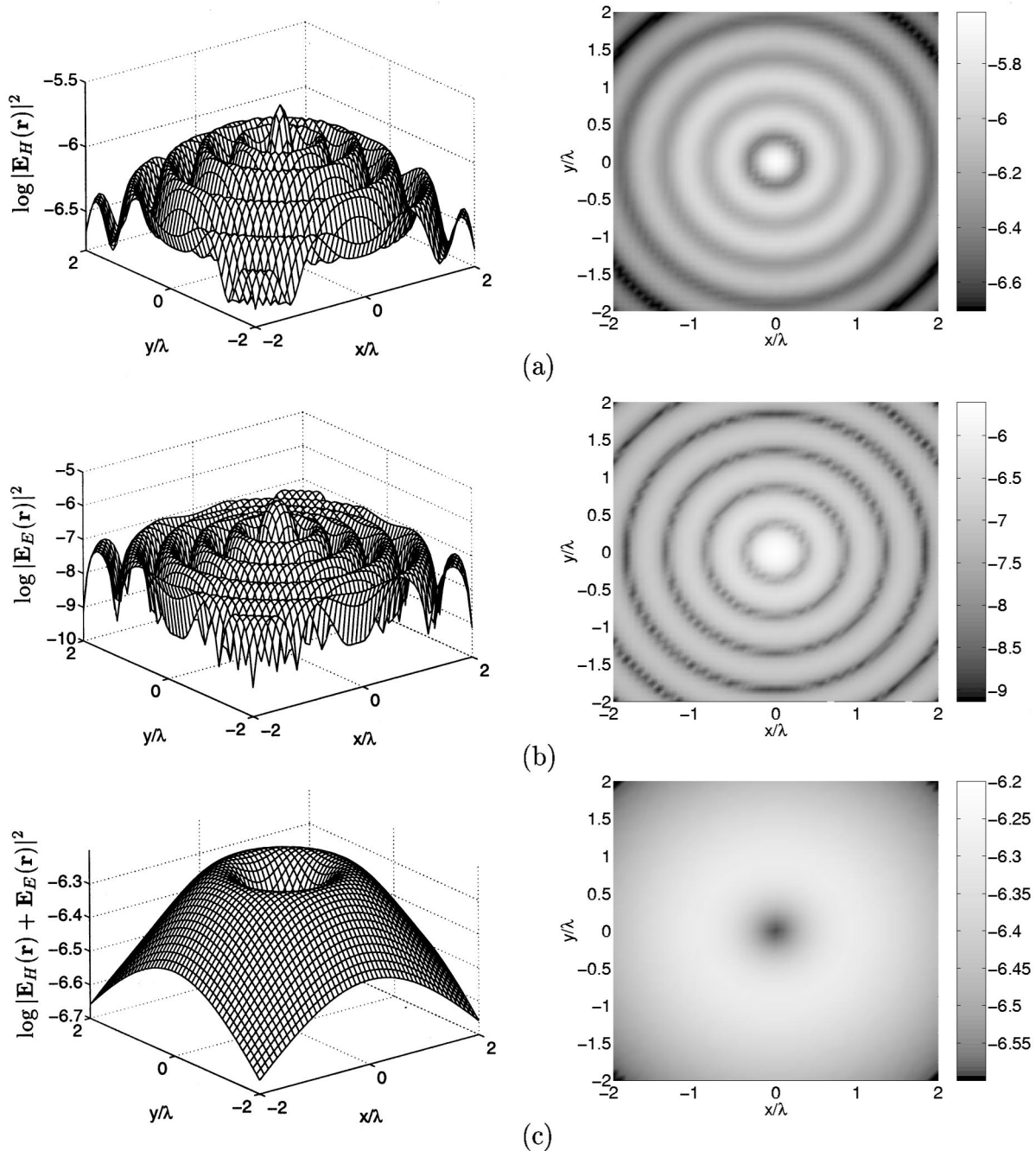
FIG. 3. Logarithmic ($\log_{10}$) electric energy distributions in the plane $z=\lambda$ for point dipole $\mathbf{P}=(0,0,1)$ at origin. (a) Homogeneous part, (b) evanescent part, (c) total field; $\lambda=633$ nm.

tion as shown in Fig. 2. The homogeneous and evanescent parts of the ensuing electric field, denoted by $\mathbf{E}_H(\mathbf{r})$ and $\mathbf{E}_E(\mathbf{r})$, respectively, are then obtained with the help of Eq. (2.1). The results, as would be observed in the planes $z=\lambda$ and $y=0$ (see Fig. 2), are illustrated in Figs. 3 and 4. More specifically, the logarithmic homogeneous and evanescent electric energy density distributions $\log_{10}|\mathbf{E}_H(\mathbf{r})|^2$ and $\log_{10}|\mathbf{E}_E(\mathbf{r})|^2$ in the plane $z=\lambda$ are plotted in Figs. 3(a) and 3(b), respectively, while Fig. 3(c) shows the logarithmic total electric energy density $\log_{10}|\mathbf{E}(\mathbf{r})|^2$. Analogous results pertaining to the plane $y=0$ are illustrated in the three parts of Fig. 4. We note that $|\mathbf{E}_H(\mathbf{r})|^2+|\mathbf{E}_E(\mathbf{r})|^2\neq|\mathbf{E}(\mathbf{r})|^2$ because of the interference terms. The fields $\mathbf{E}_H(\mathbf{r})$ and $\mathbf{E}_E(\mathbf{r})$ generated

by a point dipole are seen to have the same characteristics as the corresponding fields produced by the scalar point source (cf. Fig. 1). The homogeneous and evanescent parts exhibit sharp ridges, while the total field is smooth. As in the scalar case, the evanescent waves decay exponentially only in the $z$ direction and propagate in the plane perpendicular to it. These characteristics do not depend on the direction of the source dipole. We stress again, however, that the arguments about the physical meaningfulness of the division stated in connection with the scalar function $G(\mathbf{r})$ also apply for this vector field case.

Let us now consider the form of the evanescent Green function in the two special directions of the $z$ axis and the
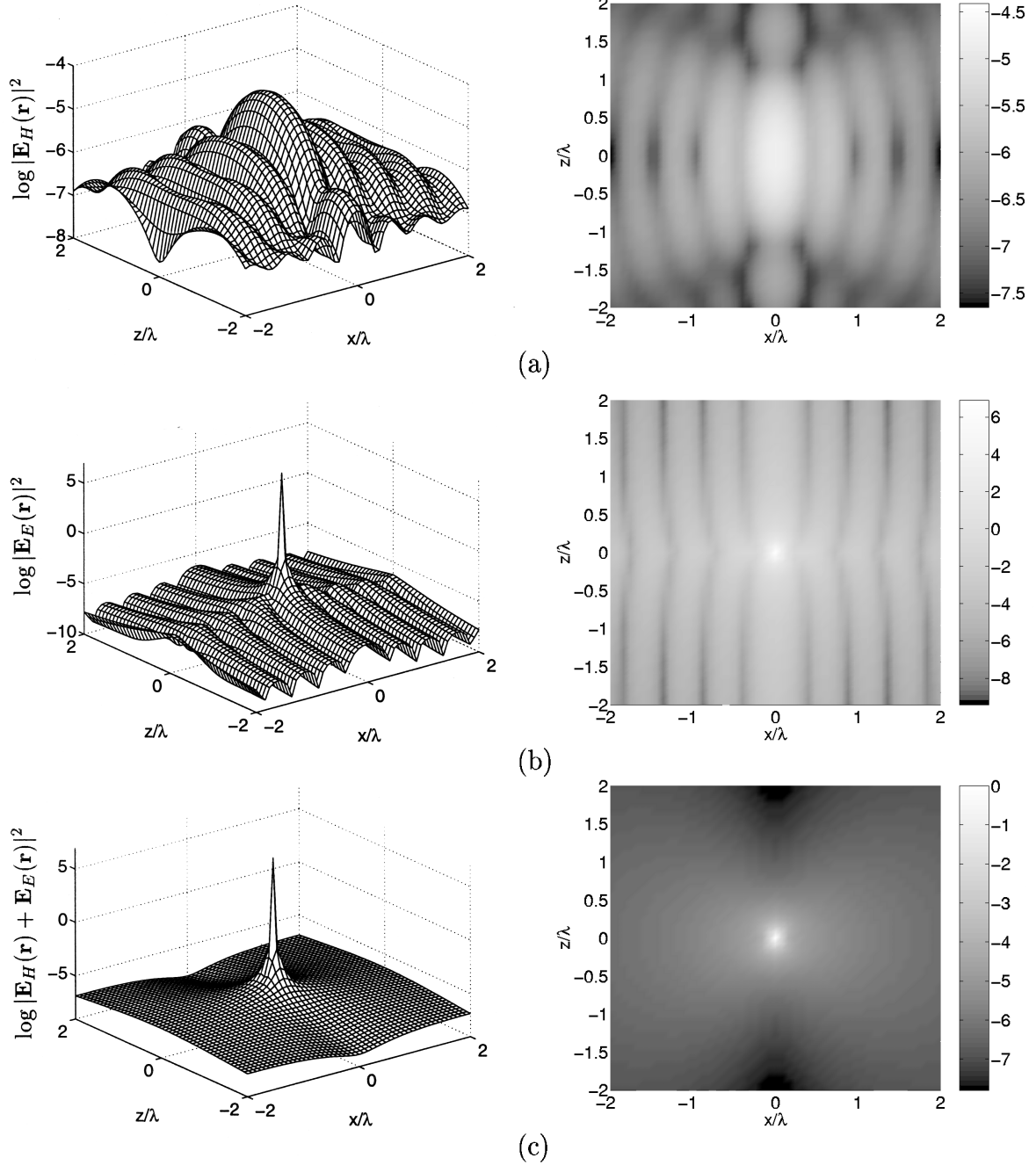
FIG. 4. Logarithmic ($\log_{10}$) electric energy distributions in the plane $y=0$ for point dipole $\mathbf{P}=(0,0,1)$ at origin. (a) Homogeneous part, (b) evanescent part, (c) total field; $\lambda=633$ nm.

$z=0$ plane. Setting $x=y=0$ in Eq. (4.1) and integrating over the evanescent waves only, it is straightforward to show that along the $z$ axis $\vec{G}_E(\mathbf{r})$ can be expressed as

$$\vec{G}_E(z)=\left(\frac{1}{2|z|}-\frac{1}{k^2|z|^3}\right)\vec{U}+\left(\frac{1}{2|z|}+\frac{3}{k^2|z|^3}\right)\mathbf{kk}, \quad (4.9)$$

where $\mathbf{k}$ is the unit vector in the $z$ direction, i.e., normal to the plane $z=0$ that divides the space into the two source-free halves. The corresponding homogeneous Green function along the $z$ axis can be calculated from $\vec{G}_H(z)=\vec{G}(z)-\vec{G}_E(z)$. Similarly, in the plane $z=0$ both the evanescent

and the homogeneous Green function can be expressed in a closed form. In this case the integrals $I_n^E$ in Eq. (4.8) reduce to

$$I_0^E(z=0)=\frac{\cos\beta}{\beta},$$

$$I_1^E(z=0)=-\frac{J_1(\beta)}{\beta}, \quad (4.10)$$

$$I_2^E(z=0)=-\frac{\sin\beta}{\beta^2}-\frac{\cos\beta}{\beta^3}.$$

With the help of Eq. (4.10) and l'Hospital's rule, one obtains for the corresponding $L_n^E$ terms

$$L_1^E(z=0) = \frac{\sin \beta}{\beta} + \frac{\cos \beta}{\beta^2},$$

$$L_2^E(z=0) = \frac{\cos \beta}{\beta} - \frac{\sin \beta}{\beta^2} - \frac{\cos \beta}{\beta^3}, \qquad (4.11)$$

$$L_3^E(z=0) = -\frac{J_2(\beta)}{\beta}.$$

In the same manner for the homogeneous part, the integrals $I_n^H$ in Eq. (4.5) in the $z=0$ plane can be expressed as

$$I_0^H(z=0) = \frac{\sin \beta}{\beta},$$

$$I_1^H(z=0) = \frac{J_1(\beta)}{\beta}, \qquad (4.12)$$

$$I_2^H(z=0) = -\frac{\cos \beta}{\beta^2} + \frac{\sin \beta}{\beta^3},$$

and the $L_n^H$ terms as

$$L_1^H(z=0) = -\frac{\cos \beta}{\beta} + \frac{\sin \beta}{\beta^2},$$

$$L_2^H(z=0) = \frac{\sin \beta}{\beta} + \frac{\cos \beta}{\beta^2} - \frac{\sin \beta}{\beta^3}, \qquad (4.13)$$

$$L_3^H(z=0) = \frac{J_2(\beta)}{\beta}.$$

By inserting expressions (4.10) and (4.11) into Eq. (4.6), one observes that, as in propagation along the $z$ axis, the evanescent Green function falls off as $1/r$ also in the $z=0$ plane. Furthermore, as a limiting case one obtains

$$\overset{\leftrightarrow}{G}_H(\mathbf{r}=\mathbf{0}) = \tfrac{2}{3} ik \overset{\leftrightarrow}{U}. \qquad (4.14)$$

This shows that the homogeneous part in the source point is finite and the singularity in the total field resides in the evanescent part.

The result along the $z$ axis, Eq. (4.9), is precisely the same (except for units and an overall minus sign) as that put forward in Refs. [6], but in those works it is claimed that this form should hold in all directions. This cannot possibly be correct. Apart from the $z$ axis and the $z=0$ plane, the leading term of the evanescent part of the spherical wave is $(kr)^{-3/2}$ [9]. One can analytically apply the differential operator of Eq. (2.2) on this asymptotic form and see that the result does not contain terms behaving as $1/kr$. This shows that except for the two special directions, the dyadic evanescent Green function falls faster than $1/kr$.

## V. CONCLUSIONS

In this work we used the known results from scalar-wave propagation and decomposed in appropriate half-spaces the dyadic free-space Green function into its homogeneous and evanescent parts. We found that properties similar to those for scalar fields are also associated with vector fields, i.e., that irrespective of the dipole orientation, the dyadic evanescent waves decay exponentially in the $z$ direction and propagate parallel to it. This result originates from the fact that the dyadic free-space Green function is generated by the corresponding scalar Green function.

Contrary to what has been proposed in the literature before, the dyadic Green-function decomposition depends on the choice of the half-spaces, in a fixed reference frame, and leads to different expressions for different choices. In any practical situation the proper half-space is determined by the physical conditions.

[1] D. Courjon and C. Bainier, Rep. Prog. Phys. **57**, 989 (1994).

[2] J. P. Fillard, *Near Field Optics and Nanoscopy* (World Scientific, Singapore, 1996).

[3] E. Wolf, in *Trends in Optics*, edited by A. Consortini (Academic, San Diego, 1996), p. 83; N. Garcia and M. Nieto-Vesperinas, Opt. Lett. **20**, 949 (1995); A. Madrazo and M. Nieto-Vesperinas, J. Opt. Soc. Am. A **14**, 618 (1997).

[4] W. H. Carter, J. Opt. Soc. Am. **65**, 1054 (1975).

[5] D. C. Bertilone, J. Mod. Opt. **38**, 865 (1991).

[6] M. Xiao, Opt. Commun. **132**, 403 (1996); Chem. Phys. Lett. **258**, 363 (1996); J. Mod. Opt. **44**, 327 (1997); Opt. Commun. **136**, 213 (1997).

[7] C.-T. Tai, *Dyadic Green's Functions in Electromagnetic Theory* (Intext, Scranton, PA, 1971).

[8] L. Mandel and E. Wolf, *Optical Coherence and Quantum Optics* (Cambridge University Press, Cambridge, 1995), Sec. 3.2.

[9] G. C. Sherman, J. J. Stamnes, A. J. Devaney, and É. Lalor, Opt. Commun. **8**, 271 (1973); G. C. Sherman, J. J. Stamnes, and É. Lalor, J. Math. Phys. **17**, 760 (1976).

[10] E. Wolf and J. T. Foley, Opt. Lett. **23**, 16 (1998).